Spring 5-2016

Increasing the Resolution of the Last Glacial Maximum Record in the Tropical Andes Using 10Be Cosmogenic Surface-Exposure Dating in the Cordillera Carabaya, Peru

Zachary E. Mason
University of Maine

INCREASING THE RESOLUTION OF THE LAST GLACIAL MAXIMUM RECORD IN THE TROPICAL ANDES USING ^{10}Be COSMOGENIC SURFACE-EXPOSURE DATING IN THE CORDILLERA CARABAYA, PERU

By

Zachary E. Mason

A Thesis Submitted in Partial Fulfillment
of the Requirements for a Degree with Honors
(Earth Sciences)

The Honors College

University of Maine

May 2016

Advisory Committee:

Brenda L. Hall, Professor of Earth and Climate Sciences and Climate Change, Advisor
Gordon R. M. Bromley, Assistant Professor, Earth and Climate Sciences, Advisor
Aaron E. Putnam, George H. Denton Assistant Professor of Earth and Climate Sciences
Amanda A. Olsen, Assistant Professor of Earth and Climate Sciences
Mark E. Haggerty, Rezendes Preceptor of Civil Engagement

Abstract

Owing to the abundance of heat and moisture, the tropics is a fundamental component of the global climate system. Yet the role of the tropics in climate remains poorly understood. The Andes are home to ~95% of all tropical glaciers, making this the ideal region for studying relationships between tropical glaciers and climate. I conducted a Beryllium-10 surface exposure dating experiment using ten quartz-bearing rock samples from a series of last glacial maximum (LGM) moraines in the Minas Tira glaciofluvial valley system, Cordillera Carabaya, Peru. The AMS measured sample dates (excluding outliers) range from 24.3 ± 0.5 ka to 19.4 ± 0.5 ka, and give an average of 22.3 ± 1.5 ka. On a first order basis, this average fits within the global LGM timescale of 23–19 ka, supporting the view of contemporaneous glaciation between the hemispheres and a globally uniform ice age. My data also align broadly with the global CO_2 record, supporting – though not confirming – the hypothesis that atmospheric CO_2 levels are closely linked to temperature changes during deglaciation.

Acknowledgements

I am very grateful for the people and organizations that helped fund this project. I would first like to thank Mr. Scott Golden and the Center for Undergraduate Research for making the analysis of the project possible. I also am grateful to the National Science Foundation for their support. I would like to extend my gratitude to the field crew that collected the samples in Peru. I owe a great amount of thanks to Gordon Bromley and Brenda Hall for being fantastic mentors and advisors for this project. I would also like to offer thanks to my committee members, Aaron Putnam, Amanda Olsen, and Mark Haggerty, for their support and contributions. Additionally, I want to thank Marty Yates and Christoper Gerbi for their assistance with the more obscure rock and mineral identifications. Furthermore, I would like to thank the professors, students, and friends in the Earth and Climate Sciences department for their general support and unwavering sense of community. Finally, I would like to thank my family for their ongoing support during all of my endeavors.

Table of Contents

List of Tables

List of Figures

1. Introduction

Why should we study glaciers and the history of their past behavior? On a first-order basis, glaciers serve as physical thermometers, advancing and retreating primarily in response to changes in atmospheric temperature. For example, during the last glacial maximum (LGM), defined as the peak of the last ice age, glaciers worldwide were more extensive than today due to lower temperatures. Determining the timing of the LGM is vital to understanding paleoclimate on both local and global scales, as well to understanding the mechanisms influencing glacier behavior. The global LGM, during which ice volume was greatest and sea level was at its lowest, occurred 23,000–19,000 years ago (23–19 ka) (*Mix et al., 2001*), yet there are important local departures from this global average that allow us to begin to assess the mechanisms by which the earth goes into and comes out of an ice age.

What drives ice ages? Astronomical, or "Milankovitch", forcing is regarded as the fundamental “pacemaker” for ice ages (*Milankovitch, 1941; Hays et al., 1976; Broecker and Denton, 1990*). Specifically, the eccentricity of Earth’s orbit, combined with the tilt and precession of its spin axis, fuels cyclical ice ages through variations in the amount of solar radiation received in each polar hemisphere. Thus, one might expect there to be an alternation between Northern and Southern Hemisphere glaciation, as the effect of precession is antiphased between the hemispheres. Yet, as Mercer (*1984*) pointed out, the pattern of LGM glaciation appears to have been broadly synchronous between the hemispheres. A primary example is the North American Laurentide Ice Sheet where, in the Great Lakes Region (~42^{o} N), the LGM was dated with radiocarbon to 23–20 ^{14}C ka (27 – 24 calendar ka) (*Dyke et al., 2002*). In the southern mid latitudes, the LGM in New

Zealand (~42.2° S) occurred over a longer period, between 27 ka and 18 ka (*Putnam et al., 2013; Kelley et al., 2014*). Nonetheless, the considerable overlap in timing of the LGM between the hemispheres contrasts with any model of antiphased glaciation. Therefore, while it is generally understood that orbital variability paces the ice age cycle, the apparent interhemispheric glacial synchrony remains a persistent problem in Earth science and has been termed the "fly in the ointment" of the Milankovitch theory (*Mercer, 1984*).

This problem has resulted in different mechanisms being proposed to explain the globally synchronous LGM and glacial termination, including atmospheric carbon dioxide (CO_2) and changes in heat transfer from ocean currents (*Broecker and Denton, 1990*). Currently, CO_2 is widely considered to be a fundamental mechanism unifying global glaciation (e.g., *Saltzmann and Maasch, 1991; Broecker, 2013; Clark et al., 2012; Shakun et al., 2015*). As a greenhouse gas, CO_2 insulates the Earth's surface by trapping outgoing infrared radiation in the lower atmosphere, resulting in a relationship between CO_2 concentration and temperature. This effect is of critical importance today, as much of the current warming is seen as a consequence of greenhouse emissions (*Yue et al., 2015*). Thus, if CO_2 truly is the fundamental driver of the ice ages, past glacier behavior, which reflects temperature change, should follow changes in carbon dioxide closely.

Over the last 22 ka, global temperatures have fluctuated broadly in concert with atmospheric CO_2 concentrations (Fig. 1) (*Petit et al., 1999; Monnin et al., 2001; Shakun et al., 2015*). For example, ice age events such as the LGM, occurred during periods with lower atmospheric CO_2 concentrations and global temperatures (Fig. 1). Nonetheless, in order to establish any causal relationship between CO_2 changes and glacial maxima, this

correlation needs to be inspected more closely using glacier records as temperature proxies.

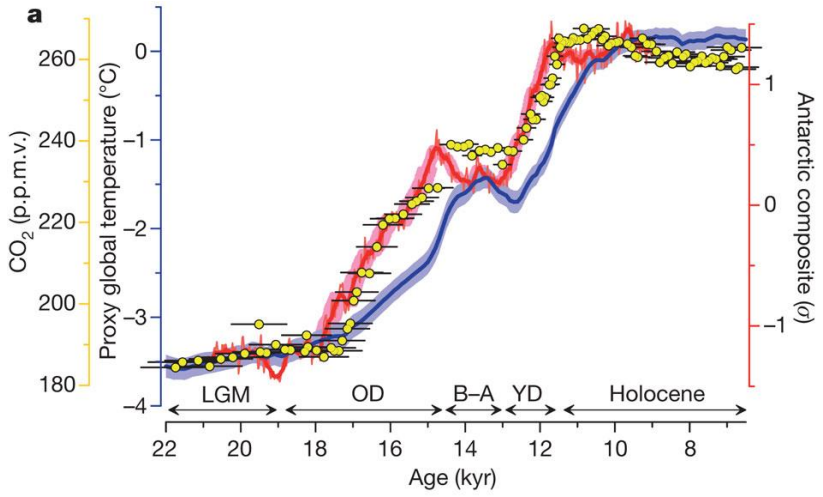

Figure 1: Comparison of changes in carbon dioxide (CO_2), global temperature, and global glaciation events since the LGM. The blue curve indicates global proxy temperature deviations from the early Holocene (11.5 – 6.5 ka) mean, the red curve shows the Antarctic ice-core composite temperature record, while atmospheric CO_2 concentrations are displayed as yellow dots. Glaciation event intervals are labeled as the Holocene, Younger Dryas (YD), Bølling-Allerød (B-A), Oldest Dryas (OD), and Last Glacial Maximum (LGM). [Figure from Shakun et al., 2012]

Owing to the strong relationship between glaciers and temperature, reconstructing past glacier behavior permits us to ascertain the timing of past climate change and how it relates (or not) to atmospheric CO_2 variations. The tropics provide us with a particularly valuable opportunity to assess this link as the tropical troposphere is characterized by thermal homogeneity and minimal seasonality (*Kaser, 1999*). Moreover, the tropics are located far from the potentially complicating effects of large mid-latitude ice sheets and steep ocean boundaries, thus resulting in glacier-temperature records that are more representative of global conditions. As the primary source of heat and water vapor, the tropics also exert a strong influence on global climate (*Cane, 1998*), emphasizing the importance of resolving the relationship between tropical temperature and CO_2.

To resolve better the potential role of carbon dioxide in the ice ages, my work provides a record of glacier behavior during the LGM from a site located in the tropical Andes of southeastern Peru. The tropical Andes contain ~2650 km^2 of glacier ice, approximately 95% of all tropical glaciers (*Kaser and Osmaston, 2002)*. Crucially, glaciers in this region have been shown to be sensitive indicators of temperature (*Rodbell et al., 2009*), thereby enabling a direct reconstruction of past temperature variability that can then be compared to possible forcing mechanisms, such as atmospheric CO_2.

2. Background

2.1 Geographic and Climatic Setting

The Andes mountains span 68º of latitude, from northern Colombia (12ºN) to southern Chile and Argentina (56ºS) (*Rodbell et al., 2009*). The tropical Andes stretch from Colombia in the north, south into Ecuador and Peru, and into Bolivia. Moisture carried by tropical easterlies travels over the Amazon Basin to the eastern side of the tropical Andes, leaving a drier western side from a rain shadow effect (Fig. 2) The Humboldt Current (Peru Current) is a cold, low-salinity ocean current flowing along the western side South America from Chile to northern Peru (*Thiel et al., 2007*) (Fig. 2). These wind circulation patterns and cold ocean currents combine to make the western side of the Peruvian Andes considerably drier than the eastern section. Correspondingly, glaciation is more extensive on the wetter eastern flanks than on the drier western side.

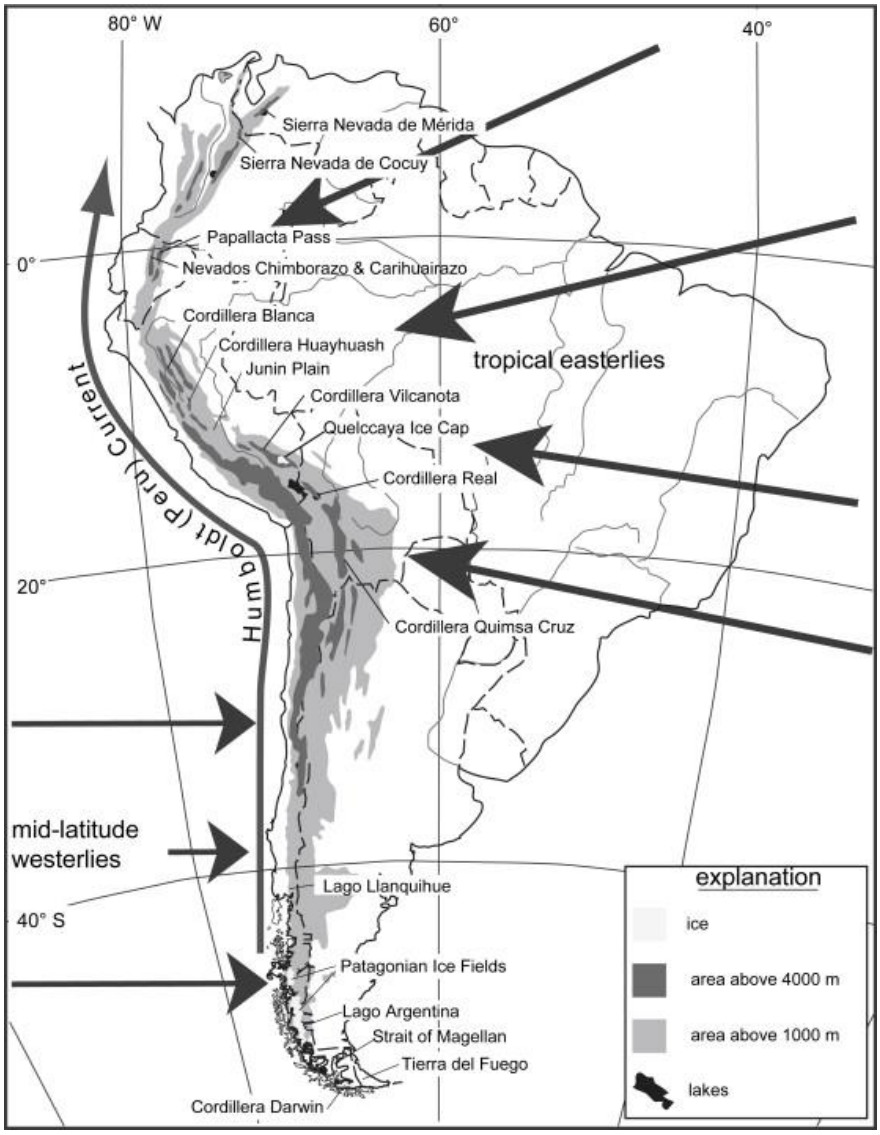

Figure 2: Map displaying South America with the many glaciated ranges of the Andes mountains. Wind patterns are shown in black arrows, while ocean currents are shown in dark gray arrows. [From Rodbell et al., 2009, which is a modified version of Clapperton, 1983]

The Peruvian Andes hold the largest proportion of all tropical glaciers (~70%), making it a primary location to research the timing of the tropical LGM (*Vuille et al., 2008*). Glaciation in Peru is extensive, currently about 2600 km^2 of ice on 20 distinct cordilleras, owing to ongoing tectonic uplift events where orogenic masses are being moved into the cryosphere (*Morales-Arnao and Hastenrath 1998; Smith et al., 2008*). The most heavily glaciated ranges include the Cordillera Blanca of central Peru, where

numerous peaks exceed 6000 m elevation (including Nevado Huascarán Sur, Peru's highest peak at 6768 m a.s.l.), and the Cordillera Vilcanota, Nevado Ausangate (6372 m), and the Quelccaya Ice Cap (*Smith et al., 2008*) in southern Peru. The Central Andean Plateau, known as the Altiplano, comprises a low-relief plain with a constant elevation of 3500–4000 m (*Smith et al., 2008)*. Current glacial limits in the tropical Andes are about 5000 m, yet terminus elevations are somewhat lower in the Cordillera Blanca, Cordillera Huayhuash, and Cordillera Vilcanota of Peru (*Frenierre et al., 2011*). In addition, Peru's Quelccaya Ice Cap is the only remaining ice cap in the entire tropical latitudes (*Frenierre et al., 2011*).

My study area is located in the Cordillera de Carabaya, a southeastern portion of the Cordillera Oriental. This mountain range occurs between 14°00'S and 14°22'S latitude and 69°38'W and 70°19'W longitude. In 1999, the Cordillera de Carabaya was measured to contain more than 100 km^2 of glacier ice (USGS, 1999). My site, Minas Tira, lies at an elevation of 4500 m with a location at 14°16'16"S latitude 70°26'42"W (Fig. 4).

2.2 Geologic Setting

The Peruvian Andes were formed by Cenozoic tectonic shortening of the South American plate margin overriding the subduction of the Nazca plate (*Sobolev and Babeyko, 2005*). This orogenic and cratonic development influenced the formation of the Cordillera de Carabaya, which is underlain by a thick succession of Phanerozoic sedimentary and volcano-sedimentary strata, as well as by a variety of intrusive units (*Sandeman and Clark*, 2004). A relatively thick (15-20 km) sequence of Ordovician to Lower Carboniferous arenites and shales is overlain by limestones, cherty sandstones,

and shales of the Middle Carboniferous to Lower Permian Tarma and Copacabana Groups (*Sandeman and Clark*, *2004*). Lower Permian strata of the Mitu Group, unconformably overlie the sequences written above and are dominated by cobble conglomerates and sandstones, with less common alkaline volcanic rocks and associated intrusive units (*Sandeman and Clark*, *2004*; *Clark et al., 1990*).

Topographically, Minas Tira comprises two adjoining valley systems Quebrada Tiratañа and Quebrada Jotini (Fig. 4) that, ultimately, drain into Lake Titicaca. The valley bottoms contain wetland and alluvial deposits incised by fluvial processes. Surficial deposits at Minas Tira include lateral and terminal moraine ridges marking the former extent of glaciers, the distribution of which indicates the former presence of two separate ice tongues. Moraines are absent for several kilometers up-valley of Minas Tira.

2.3 Previous Work in the Tropical Andes

Here, I discuss some of the previous LGM research that has been conducted in the tropical Andes, primarily in Ecuador, Peru, and Bolivia. It is important to note that there has been an abundance of published research regarding the timing of the LGM in this region, along with a variety of dating techniques including radiocarbon and surface exposure-age dating (Fig. 3). Therefore I shall focus on a representative body of prior research in order to maintain brevity.

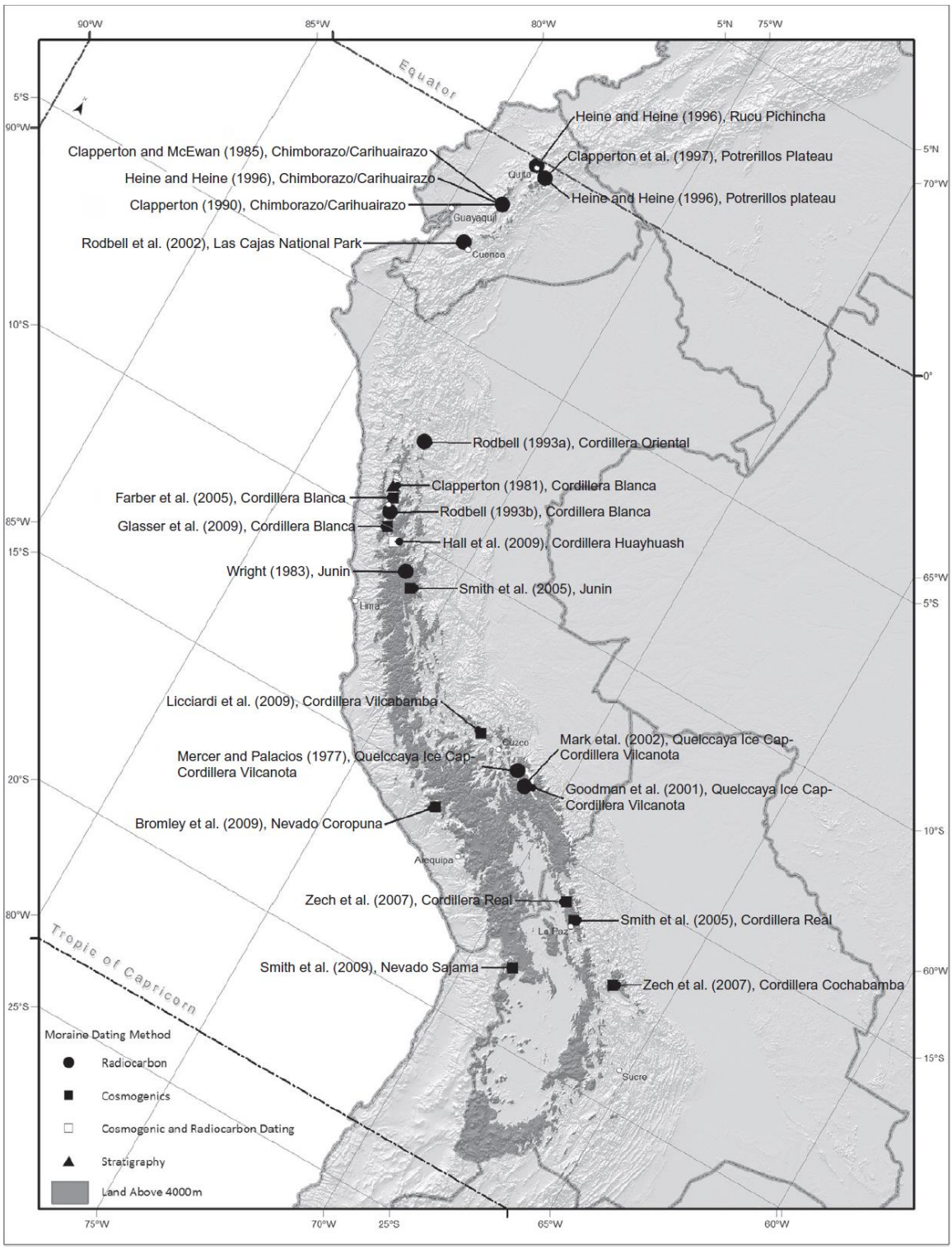

Figure 3: Map displaying a compilation (pre-2011) of collected radiocarbon and surface exposure-age dating data of glacial moraines throughout the tropical Andean region in Ecuador, Peru, and Bolivia. [From Frenierre et al., 2011]

In Ecuador, Heine and Heine (*1996*) dated seven distinct moraine groups near Rucu Pinchinca (Fig. 3) and Papallacta Pass and labeled them from oldest (M1) (Middle Pleistocene) to youngest (M7) (Early–Middle Holocene), with M4 interpreted as the LGM moraine. M4 moraines were found at around 3800 to 3900 m elevation (*Heine and Heine 1996*). Heine (*2000*) suggested that the M4 moraines represent relatively restricted LGM glaciers. The radiocarbon dates along with geomorphological and paleopedologic evidence, together with dated tephras erupted from Pichincha volcano, provided moraine ages younger than 30 ^{14}C ka, culminating sometime around 28 ^{14}C ka (approximately 40 – 33 ka calendar years). These results suggest an early local last glacial maximum (LLGM) in Ecuador.

In Peru, Bromley et al. (*2009*) applied cosmogenic ^{3}He surface exposure-age dating to samples from LGM moraines on Nevado Coropuna (Fig. 3). Their results have produced a timing range of about 25 – 15 ka with a mean age of around 20.7 ± 3.7 ka (*Bromley et al., 2009*). Smith et al. (*2005*) claimed a possible early LLGM in the Peruvian Andes, with data from central Peru. Their ^{10}Be surface exposure-age data from LGM moraines in the Junin valleys (Fig. 3) suggested maximum ice extent at between 34 – 22 ka (*Smith et al., 2005*). Seltzer et al. (*1990, 2000*) used paleoclimate proxies, such as magnetic susceptibility and radiocarbon dating from stratigraphic records from the Junin Lake and Lake Titicaca, to bracket the LLGM to between 30 – 21 ka.

In Bolivia, Zech et al. (*2007*) used ^{10}Be surface exposure-age dating on 28 boulders from the LGM moraines in Cordillera Real and the Cordillera Cochabamba (Fig. 3). These dates range from 25 to 22 ka, suggesting a near-synchronous LLGM in Bolivia to the global average of 23 – 19 ka. Similarly, extensive surface exposure dating

in the Bolivian Andes conducted by Smith et al. (*2005*) also claimed an early LLGM there, with ^{10}Be data from LGM moraines in the Cordillera Real (Fig. 3) and the Miluni Valley ranging from 34 to 23 ka (*Smith et al., 2005*).

At face value, this wealth of data from previous studies suggests the timing of the LGM in the tropical Andes is already well understood. However, there are several key limitations to consider when approaching the existing data set. Although radiocarbon dating can be implemented to bracket age constraint, moraine elevations in the tropical Andes are typically too high for vegetation to grow. The relative dearth of organic material for dating ultimately produces low-resolution ^{14}C records. In contrast, surface-exposure dating, which does not rely on organic material, has greatly improved opportunities for constraining moraine age. However, the majority of the cosmogenic studies described above were conducted when the technique was still in its infancy and thus of relatively low resolution. For example, only recently has the ^{10}Be production rate been calibrated for low-latitude, high-altitude sites, such as the Peruvian Andes (*Kelly et al., 2015*). Previous studies had to rely on estimates of production rate. Additionally, there have been improvements in sampling procedures and in the handling of data, which implies that current data in the tropical Andes must be observed through a lens of greater uncertainty. Consequently, my work aims to add clarity to our understanding of the timing of the LGM in this region.

3. Methods

I used cosmogenic ^{10}Be surface-exposure dating to constrain the ages of ten quartz-bearing boulder samples (n = 10) from Minas Tira to achieve ages of moraines, in

order to bracket the timing of the LGM in the tropical Peruvian Andes. This area was selected as a part of a project funded initially by the Natural Science Foundation (NSF) to help establish the role of the tropics in global climate. In 2011, a team led by Gordon Bromley conducted field mapping and sampling (I did not participate in this section of the project). They identified relict lateral and terminal moraines, along with erosional glacial landforms throughout both the Tiratańa and Jotini drainages, and grouped deposits on the basis of position, weathering, and elevation. Bromley used this information subsequently to produce a glacial geomorphic map showing former ice-age extents of glaciers at Minas Tira (Fig. 4). This map forms the basis for establishing my glacial chronology.

Samples for cosmogenic ^{10}Be surface-exposure dating were collected from suitable erratics on moraine crests based on the quality of each boulder's positioning, stability, and quartz concentration. Boulders were also observed for striations or other evidence of glacial erosion, and were preferentially selected on minimal evidence of post-depositional erosion and weathering. Bromley sampled only boulders greater than 1 m in relief to lessen the possibility of shielding effects from snow or vegetation and each erratic was described in context, photographed, and their GPS locations documented. Rock samples of the upper few centimeters (1-2 cm) from chosen boulders were gathered with hammer and chisel. Additionally, the group measured the horizon with a clinometer to calculate the cosmic ray flux, accounting for any topographic factors that affected shielding. Subsequently, samples were taken back to the Climate Change Institute at the University of Maine to be prepared for ^{10}Be extraction.

Here, I discuss a brief summary of my part in preparing samples in the laboratory for ^{10}Be extraction, following the methods described by Schaefer et al. (*2009*) (Steps in Appendix A). I initially selected ten, high-quality samples, using criteria similar to those for the selection of boulders written above, from the moraine belts in the Quebrada Tirataña that would provide a spread of time in bracketing the LGM. I then documented each sample's rock type and quartz content and measured their masses on a digital scale. To reduce grain size of each sample, I crushed and pulverized the rocks. I used a set of sieves to sort out the samples by grain sizes, and used a fraction of 250 μm to 500 μm range for further processing. This fraction for each sample was washed with water in order to remove dust, and then were boiled in a 6 molar hydrochloric acid solution to remove adhering clays and oxides. Samples were dried. In order to separate quartz from the other minerals present (e.g., feldspar), I first tried a froth floatation method designed to float feldspars so that quartz could collected (*Science.purdue.edu, 2016*). However, this success of this method can be highly variable, depending on lithology and in this case it was unsuccessful, so I instead separated the quartz based on density differences using heavy liquids. Any magnetic minerals left with the quartz were removed using the Frantz machine. By this point my samples consisted of nearly pure quartz. Visual examination under the microscope revealed trace amounts of crystalline feldspar, which were removed by hand. Samples were then etched in 2% hydrofluoric acid for a week for final quartz clean up. Samples were then taken to a clean laboratory for Be extraction. Each sample was weighed, and a ^{9}Be carrier was added, including to a blank, before the quartz was dissolved in concentrated hydrofluoric (HF) acid. I put each sample (including the blank) through cation and anion exchange columns in order to remove contaminating elements,

such as Fe, Ca, and Ti (*Ditchburn et al., 1994; Ditchburn et al., 2000*). I then precipitated the beryllium as a hydroxide, which I combusted to convert to beryllium oxide. I packed all of the samples into cathodes, which were then sent to the Lawrence-Livermore CAMS facility for ^{10}Be to ^{9}Be ratio measurements. Beryllium ratios in samples and blanks were measured relative to the 07KNSTD standard, where $^{10}Be/^{9}Be = 2.85 \times 10^{-12}$ (*Nishiizumi et al., 2007*).

I calculated the surface-exposure ages using the CRONUS-Earth online calculator, version 2.2 (*Balco et al., 2008*), after receiving the ^{10}Be to ^{9}Be ratio measurements from Lawrence-Livermore National Laboratory. These calculations were completed using the most recent local ^{10}Be production rate provided by Kelly et al. (*2015*) and the time-independent 'St' scaling (*Lal, 1991; Stone, 2000*). This scaling method allows the production rate taken from the nearby Quelccaya Ice Cap (*Kelly et al., 2015*) to be used at our site at Minas Tira, by adjusting it for physical differences between localities (i.e. altitude, position, pressure, etc.). The 'St' scaling protocol is also considered the most accurate for the tropics (*Kelly et al., 2015*).

4. Results

Retreat of the Tiratańa glacier since the LGM, left three prominent parallel lateral moraines on the western valley wall of the Quebrada Tiratańa. The moraines diverge southwards towards the terminus, into several terminal ridges within three well-defined belts. The belts contain ridges with about 2-5 m in relief and are separated by valleys that are approximately 10 m wide. The ridges of this complex show identifiable moraine

features consisting of strong crest shapes along with prominent ice-contact slopes, which are scattered with granitoid, sandstone, conglomerate, and ignimbrite boulders.

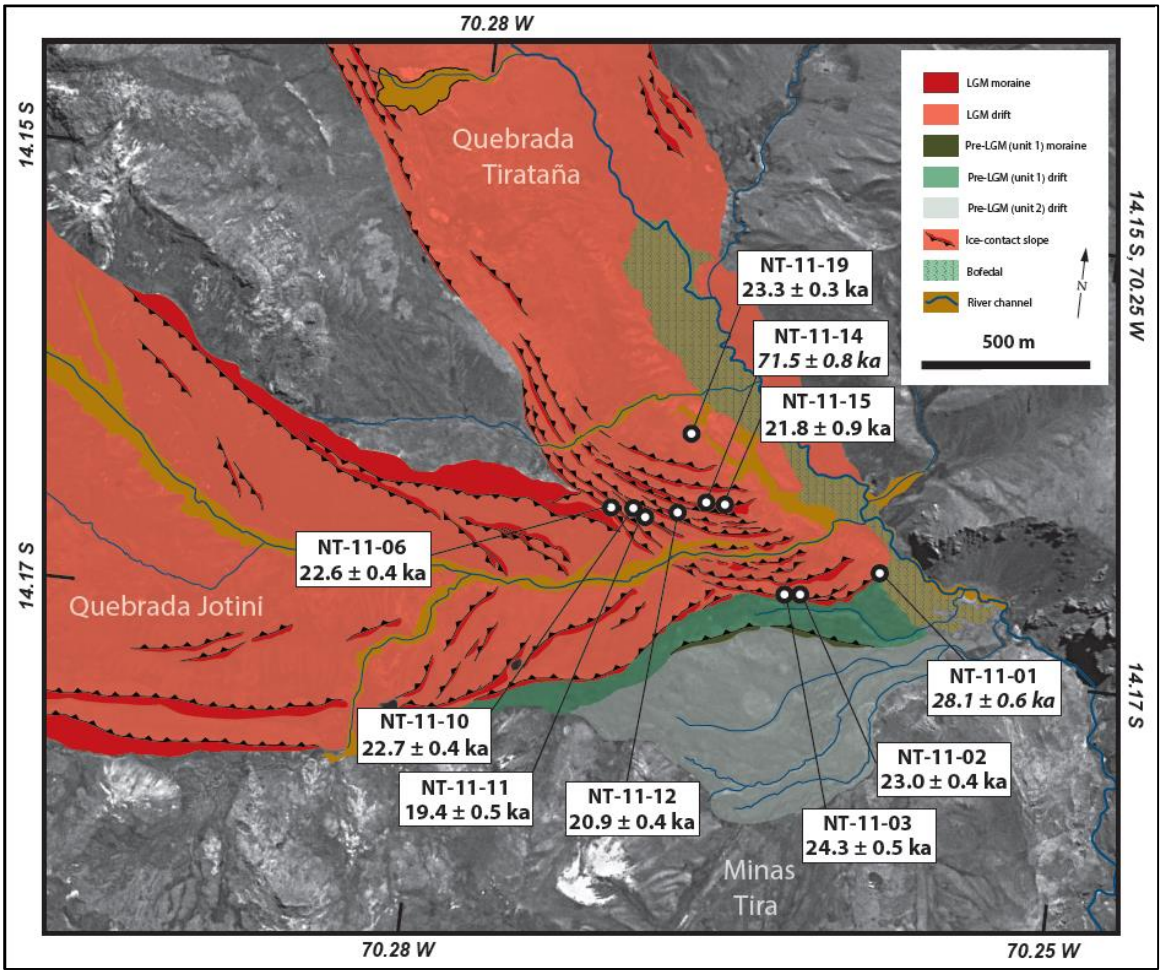

Figure 4: Map display of Minas Tira within the Cordillera de Carabaya, Peru. The two valley systems, Quebrada Tirataña and Quebrada Jotini, are shown along with their corresponding lateral and terminal moraines. Samples (n=10) come from the Quebrada Tirataña valley terminal moraine belts, and are marked with accompanying sample names and calculated ^{10}Be surface-exposure ages. Both samples NT-11-01 and NT-11-14 have their ages italicized, as they are regarded as outliers.

We sampled ten boulders from the terminal moraine complex in the Quebrada Tirataña. Our sampled boulders showed minor amounts of weathering in the form of discoloration and shallow weathering pits only measuring a few millimeters deep, along with visible glacial erosion evident from minor striations and polish. Samples NT-11-01, 02, and 03 were collected in the outermost southeastern portion of the LGM terminal moraine belts, and they achieved ages in the range of 28.1 ± 0.6 ka to 23.0 ± 0.4 ka (Fig. 4). NT-11-06 was collected on western section of the outermost ridge in the Tirataña valley, with samples NT-11-10 and NT-11-11 gathered nearby (Fig. 4). This group has ages ranging from 22.7 ± 0.4 ka to 19.4 ± 0.5 ka. Samples NT-11-12 and NT-11-15, from a more proximal position, produced ages of 20.9 ± 0.4 ka and 21.8 ± 0.9 ka, respectively (Fig. 4). NT-11-14 was sampled from the same moraine as NT-11-15. However, NT-11-14 is regarded as an outlier as the sample had a considerably older age of 71.5 ± 0.8 ka. The innermost, up-valley sample (NT-11-19) produced an age of 23.3 ± 0.3 ka.

Table 1.
Minas Tira moraine sample attributes and ^{10}Be surface-exposure ages. All exposure ages were calculated using the tropical high-altitude production rate of Kelly et al. (2015) and St scaling (Lal, 1991; Stone, 2000), rock density of 2.7 g/cm^3, and zero erosion. Beryllium ratios of samples and blanks were measured relative to the 07KNSTD standard [^{10}Be/^{9}Be = 2.85×10^{-12}]. NT-11-01 and NT-11-14 are italicized as they are considered outliers.

Sample	Latitude	Longitude	Altitude (m)	Thickness (cm)	Horizon correction	^{10}Be concentration (10^5 atoms/g)	Exposure age (ka)
NT-11-01	*-14.16354*	*-70.26168*	*4526*	*1.00*	*0.992*	*10.545 ± 0.240*	*28.071 ± 0.6*
NT-11-02	-14.16417	-70.26357	4540	1.06	0.991	8.651 ± 0.143	22.989 ± 0.4
NT-11-03	-14.16415	-70.26368	4541	1.20	0.991	9.126 ± 0.201	24.290 ± 0.5
NT-11-06	-14.16158	-70.27045	4604	1.50	0.997	8.748 ± 0.168	22.562 ± 0.4
NT-11-10	-14.16156	-70.26956	4588	1.50	0.999	8.770 ± 0.166	22.728 ± 0.4
NT-11-11	-14.16189	-70.26817	4570	0.64	0.999	7.160 ± 0.337	19.439 ± 0.5
NT-11-12	-14.16192	-70.26713	4562	1.10	0.999	8.006 ± 0.158	20.914 ± 0.4
NT-11-14	*-14.16130*	*-70.26697*	*4559*	*1.60*	*0.999*	*26.876* ± 0.296	*71.522* ± 0.8
NT-11-15	-14.16121	-70.26668	4555	1.15	0.999	8.325 ± 0.333	21.831 ± 0.9
NT-11-19	-14.15710	70.26973	4539	1.50	0.997	8.795 ± 0.098	23.349 ± 0.3

5. Discussion

Collectively, my ages from the Minas Tira moraine complex range from 71.5 ± 0.8 ka to 19.4 ± 0.5 ka. However, given that sample NT-11-14 gives an age (71.5 ± 0.8 ka) that is well over two standard deviations from the mean (Fig. 5), I reject it as an old outlier. It likely has experienced previous exposure to cosmic rays. Similarly, the age distribution curve for the four samples from the outermost terminal moraine (samples NT-11-01, 02, 03, and 06) distinguishes sample NT-11-01 (28.1 ± 0.6 ka) as a probable outlier (Fig. 6). Thus, with NT-11-14 and NT-11-01 both removed from the data set, the mean age for all remaining samples is 22.3 ± 1.5 ka, whereas that of the outermost terminal moraine is 23.3 ± 0.9 ka.

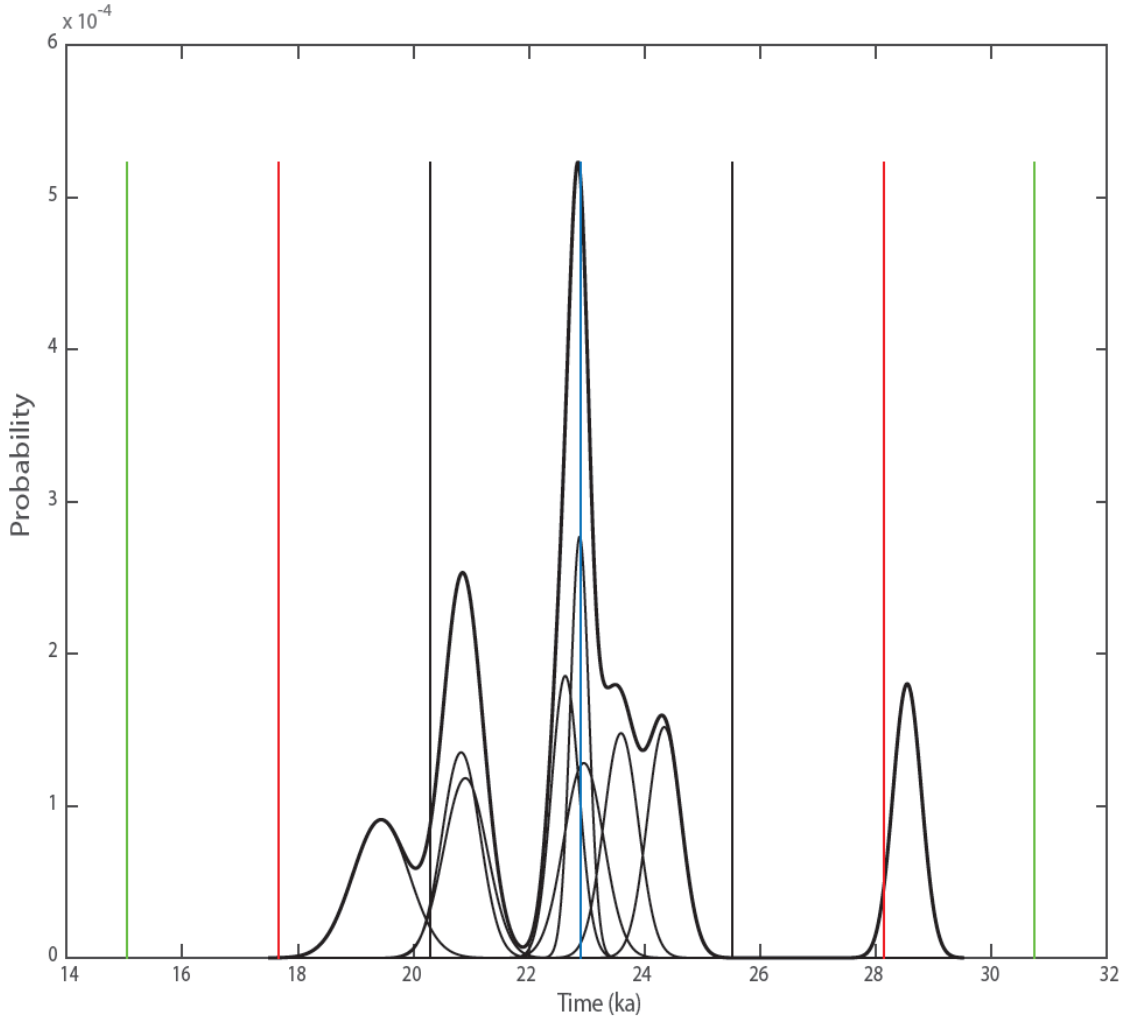

Figure 5: Probability density function (i.e., 'camelplots') for the moraine complex in Minas Tira. Center blue line is the arithmetic mean. The black, red, and green vertical lines represent uncertainties in the 1σ, 2σ, 3σ ranges respectively. Thin-lined curves are Gaussian curves representing each sample, while the thick-lined curve is the probability distribution summation of the data. Sample NT-11-14 is not shown as it falls well beyond 2σ of the distribution, and it is distinguished as an outlier.

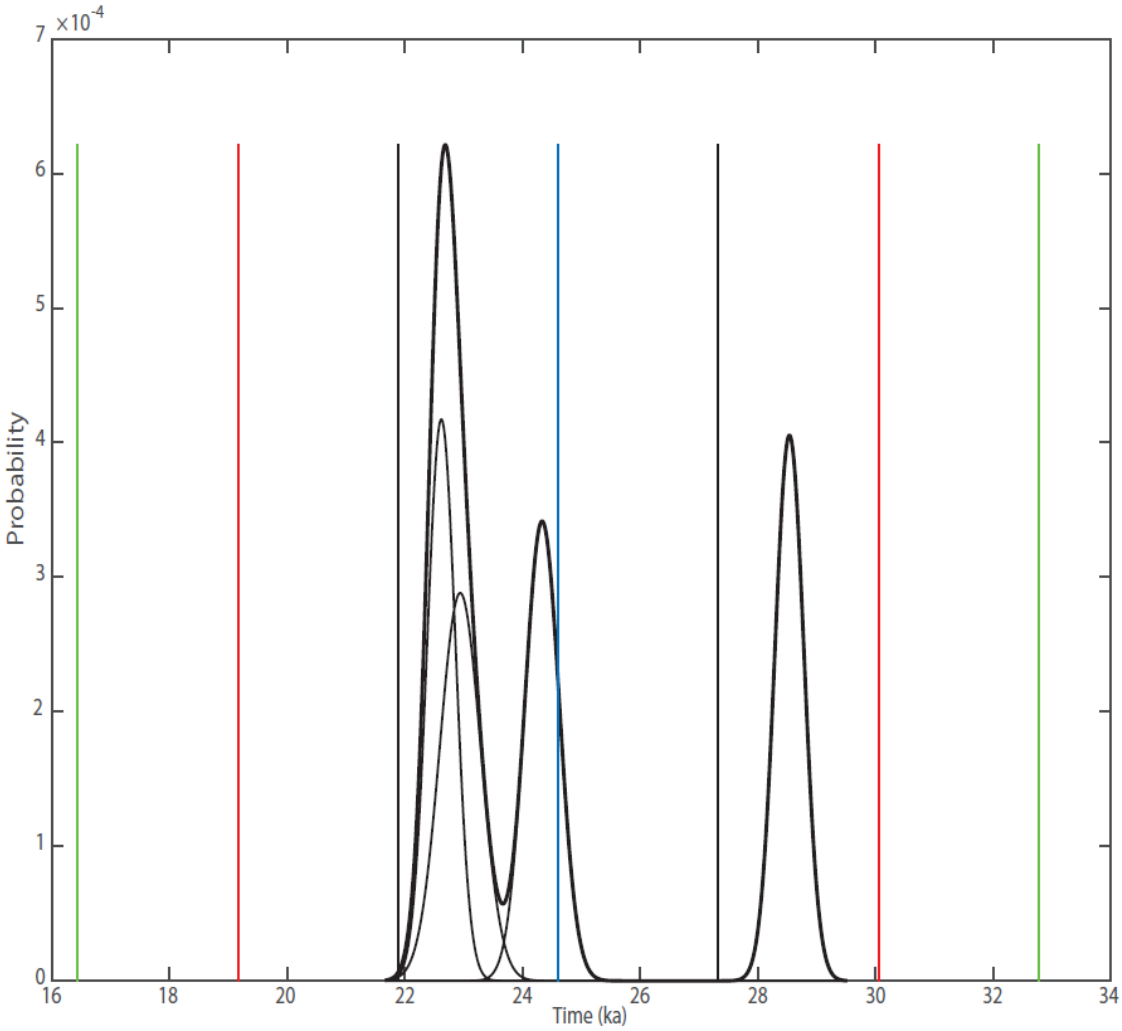

Figure 6: Probability density function (i.e., 'camelplots') for the outermost moraine in the sampled Minas Tira complex, including four samples (NT-11-01, 02, 03, and 06). Center blue line is the arithmetic mean. The black, red, and green vertical lines represent uncertainties in the 1σ, 2σ, 3σ ranges respectively. Thin-lined curves are Gaussian curves representing each sample, while the thick-lined curve is the probability distribution summation of the data. The oldest curve shown is sample NT-11-01, which is recognized as an outlier.

Due to the relatively low number of samples from each of the inner moraine ridges, it is not feasible to assess their ages statistically as I have for the outer moraine. Nonetheless, it is important to assess the quality of the dates as a single unit and as a sequence in time. Stratigraphically, the outer moraine ridge should be the oldest, representing the most extensive position of the glacier during the LGM, whereas

subsequent moraines should be progressively younger with distance up-valley. On a first-order basis, this pattern is somewhat evident in my data set. For example, samples NT-11-10, 11, 12 and 15 all give ages younger than the average of the outermost moraine and are located inboard of that limit (Fig. 4). However, upon closer inspection, the distribution of these four samples does not entirely fit the chronologic sequence anticipated from moraine stratigraphy. This may be due to the relatively small number of samples from each moraine, which precludes an examination of the distribution of boulder ages within a single ridge. Furthermore, the close agreement among these four recessional ages may indicate that the Minas Tira moraine complex was deposited over a short period of time that cannot be distinguished within the resolution of this dating method.

The variability among my surface-exposure ages potentially reflects a number of external factors, including inheritance of ^{10}Be due to prior exposure and perturbed exposure due to factors such as boulder exhumation, rolling, or shielding by snow. Variability might also be attributed to internal factors, such as uncertainties associated with sample preparation and accelerator mass spectrometry. However, the standard uncertainties of my ages are relatively low, indicating that any variability is unlikely to reflect errors during sample preparation.

NT-11-19 (23.3 ± 0.3 ka), collected from a position proximal to the inner moraine, is older than I would expect given its stratigraphic position. Although NT-11-19 is not a statistical outlier, I suspect that if one collected more samples at the same location, it would be older than its neighbors. It is noteworthy that both sample 19 and 14, which has already been excluded as an outlier, are composed of the same rock type. I

determined that they were quartz-bearing, sandy, carbonate conglomerates, and that this lithology is extremely resistant to mechanical erosion (as indicated by the preservation of striations and glacial polish). Thus, a potential explanation for their relatively old ages is that samples 14 and 19 were exposed previously to cosmic rays and underwent insufficient glacial erosion to reset their ^{10}Be concentrations. Consequently, this inherited beryllium produced exposure ages greater than their deposition ages. While I cannot test this hypothesis within the present study, it leaves us with a plausible model for why these two ages are older than expected.

Does the measured sample age bracket from Minas Tira fit within the timeline of the global LGM? Excluding proposed outliers, the range of dates is 24.3 ± 0.5 ka to 19.4 ± 0.5 ka, which fits within Marine Isotope Stage 2 (MIS2; 26–19 ka), supporting the view that maximum ice extent occurred during the Late Pleistocene (*Bromley et al., 2009; Clark et al., 2009*). My exposure ages also align with the global LGM, which occurred between 23 and 19 ka (*Mix et al., 2001*), and thus broadly support the paradigm of globally-synchronous glaciation.

My Minas Tira data set also agrees with many existing tropical records. For example, ^{10}Be surface exposure-age data from the Cordillera Real and Cordillera Cochabamba, Bolivia, indicate the LGM occurred there 25–22 ka (*Zech et al., 2007*). Similarly, Bromley et al. (*2009*) used cosmogenic ^{3}He surface exposure-age dating to constrain LGM moraines at Nevado Coropuna, SW Peru, to between 25 and 21 ka (recalculated using appropriate scaling; G. Bromley, personal communication, 2016). This range is broadly consistent with my Minas Tira results. More recently, a new ^{10}Be

moraine chronology for the SE Peruvian Andes suggests the LGM there occurred 28–19 ka (*Bromley et al., in review*), a timeframe that also aligns well with my data set.

Conversely, there are several bracketed LGM chronologies from tropical Andean sites that do not coincide closely with my data. For example, Smith et al. (*2005*) conducted an extensive ^{10}Be surface exposure-age study of Late Pleistocene moraines in the Junin valleys of Peru and concluded that maximum ice extent occurred there as early as 30 ka (using recalculated ages from *Bromley et al., in review*), prior to the global LGM. Similarly, Seltzer et al. (*1990, 2000*) used magnetic susceptibility and radiocarbon dating of lacustrine sediments in nearby Lake Titicaca to constrain the age of maximum glacier extent to between 30 and 21 ka. The studies above (*Smith et al., 2005; Seltzer et al., 1990, 2000*) show that glaciers possibly reached maximum volume in the tropical Andes either in the early part of the MIS2, or pre-MIS2. My data do not fit this view. Potential reasons for the difference in chronology between data sets may include the large uncertainties associated with those earlier studies, as well as improvements in sampling protocol.

Comparison of my record with similar glacial studies from the northern and southern hemispheres yields information on the global phasing of the LGM. For instance, in Chile, Denton et al. (*1999*) used radiocarbon methods to produce a chronology of the LGM moraines in the region of the southern Lake District, Seno Reloncaví, and Isla Grande de Chiloé. They found several advances between the time period of 33.5 ka and 18 ka. In the Southern Alps of New Zealand, Putnam et al. (*2013*) obtained ^{10}Be ages within the range of 32.5 ka and 18.2 ka for moraine belts near Lake Ohau. Additionally, Doughty et al. (*2015*) pieced together a ^{10}Be exposure-age chronology for LGM moraines

in the adjacent Pukaki Basin, where regional glacial maxima were achieved at various times between 41.8 ka and 18.3 ka. My exposure ages from Minas Tira do not show evidence of an earlier maximum as found in the Chilean data set, as well as in both of the data sets from New Zealand. However, the Minas Tira ages do overlap with the younger portions of the chronologies developed in these other Southern Hemisphere sites.

There are few, well-dated Northern Hemisphere records from mountain glaciers, with which to compare my data. Pendelton et al. (*2015*) did ^{10}Be exposure dating on LGM terminal moraines in the central Brooks Range of Alaska, and found a culmination period that lasted from 21 ka to somewhere in between 16 ka and 15 ka. The ages from this study mostly coincide with the Minas Tira ages. Overall, the lack of well-dated Northern Hemisphere mountain glacier records dating to the LGM is a limiting factor in making global comparisons of moraines.

Within the limitations of the record, the relative synchronicity of the LGM chronology between both hemispheres urges us to find a viable explanation for globally contemporaneous glaciation. Because insolation variations due to precession are antiphased between the hemispheres, glaciation should be asynchronous. Yet, data appear to suggest generally synchronous glaciation. This observation has become known as the "fly in the ointment" in Milankovitch's theory (*Mercer, 1984*). Therefore, the next step in my research is to investigate potential factors that would lead to synchronizing glaciation between the hemispheres. Atmospheric greenhouse gas concentrations (e.g. CO_2) are commonly cited as potential unifiers (*Saltzmann and Maasch, 1991; Broecker, 2013; Clark et al., 2012; Shakun et al., 2015*). Global temperatures, correlating strongly with glacier advance and retreat, have fluctuated broadly in concert with atmospheric CO_2

concentrations since the LGM (Fig. 1) (*Petit et al., 1999; Monnin et al., 2001; Shakun et al., 2015*). Thus, atmospheric CO_2 concentrations could very well be the factor in globally synchronous glaciation. However, the results from Minas Tira do not offer any conclusive information on this hypothesis because of the relatively low resolution of data. In order to test whether atmospheric CO_2 plays an important role in global glaciation, much higher resolution data on the timing and structure of the LGM is needed in both hemispheres.

6. Conclusion

My ^{10}Be exposure ages (excluding outliers) from samples collected on a terminal moraine complex in Minas Tira, within the Cordillera Carabaya of Peru, range from 24.3 ± 0.5 ka to 19.4 ± 0.5 ka, and give an average of 22.3 ± 1.5 ka. This bracket and average fit within the Marine Isotope Stage 2 (MIS2; 26–19 ka), and overlap the accepted global LGM of 23 – 19 ka (*Mix et al., 2001*). This chronology from Minas Tira also roughly agrees with ages from nearby studies, as well as ages from studies completed in both the Southern and Northern Hemispheres.

On a first-order basis, my results support the view of a globally synchronous LGM. This increases existing evidence for global synchrony of glaciation and supports Mercer's (*1984*) "fly in the ointment" of Milankovitch theory. There must be some fundamental component in the global climate system that unifies glaciation among both hemispheres. Atmospheric CO_2 concentration levels are broadly in concert with fluctuations of global temperatures and have been proposed to be a unifying component in global glaciation (*Saltzmann and Maasch, 1991; Broecker, 2013; Clark et al., 2012;*

Shakun et al., 2015). My data from Minas Tira are consistent with this view, however much more high-resolution data are needed from both hemispheres to confirm this relationship.

References

Arnao, Benjamin Morales, and Stefan L. Hastenrath., 1998. Glaciers of Perú. Geological Survey Professional Paper 1386, 147.

Balco, G., Stone, J., Lifton, N., Dunai, T., 2008. A complete and easily accessible means of calculating surface exposure ages or erosion rates from ^{10}Be and ^{26}Al measurements. Quaternary Geochronology 3, 174-195.

Broecker, W., 2013. What Drives Glacial Cycles? Eldigio Press, New York.

Broecker, W., Denton, G., 1990. What drives glacial cycles? Scientific American 262, 42-50.

Bromley, G.R., et al., A cosmogenic 10Be chronology for the local last glacial maximum and termination in the Cordillera Oriental, southern Peruvian Andes: Implications for the tropical role in global climate. In review for Quaternary Science Reviews

Bromley, G.R., Schaefer, J.M., Winckler, G., Hall, B.L., Todd, C.E. and Rademaker, K.M., 2009. Relative timing of last glacial maximum and late-glacial events in the central tropical Andes. Quaternary Science Reviews, 28(23), 2514-2526.

Cane, M., 1998. A role for the tropical Pacific. Science 282, 59-61.

Clapperton, C.M., 1983. The glaciation of the Andes. Quaternary Science Reviews, 2(2), 83-155.

Clark, A.H., Kontak, D.J. and Farrar, E., 1990. The San Judas Tadeo W (-Mo, Au) deposit; Permian lithophile mineralization in southeastern Peru. Economic Geology, 85(7), 1651-1668.

Clark, P. U., et al., 2012. Global climate evolution during the last deglaciation. Proceedings of the National Academy of Science 109, 1134–1142.

Clark, P.U., Dyke, A.S., Shakun, J.D., Carlson, A.E., Clark, J., Wohlfarth, B., Mitrovica, J.X., Hostetler, S.W. and McCabe, A.M., 2009. The last glacial maximum. science, 325(5941), 710-714.

Denton, G.H., Heusser, C.J., Lowel, T.V., Moreno, P.I., Andersen, B.G., Heusser, L.E., Schlühter, C. and Marchant, D.R., 1999. Interhemispheric linkage of paleoclimate during the last glaciation. Geografiska Annaler: Series A, Physical Geography, 81(2), 107-153.

Ditchburn, R. G. and N. E. Whitehead., 1994. The separation of 10Be from silicates. 3d Workshop of the South Pacific Environmental Radioactivity Association, 4-7.

Ditchburn, R. G., I. J. Graham, and A. Zondervan., 2000. Analytical methods for measuring Be and U-Th isotopes in loess. Institute of Geological and Nuclear Sciences science report 2000/09. Lower Hutt: Institute of Geological and Nuclear Sciences. 10p.

Doughty, A.M., Schaefer, J.M., Putnam, A.E., Denton, G.H., Kaplan, M.R., Barrell, D.J., Andersen, B.G., Kelley, S.E., Finkel, R.C. and Schwartz, R., 2015. Mismatch of glacier extent and summer insolation in Southern Hemisphere mid-latitudes. Geology, 43(5), 407-410.

Dyke, A. S., et al., 2002. The Laurentide and Innuitian ice sheets during the last glacial maximum. Quaternary Science Reviews 21, 9-31.

La Frenierre, J., Huh, K.I., Mark, B.G., 2011. Ecuador, Peru and Bolivia: Quaternary Glaciations—Extent and Chronology—A closer look, Developments in Quaternary Sciences 15, 773-802.

Hays, J.D., Imbrie, J. and Shackleton, N.J., 1976, December. Variations in the Earth's orbit: pacemaker of the ice ages. American Association for the Advancement of Science.

Heine, K., 2000. Tropical South America during the Last Glacial Maximum: evidence from glacial, periglacial and fluvial records. Quaternary International, 72(1), 7-21.

Heine, K. and Heine, J.T., 1996. Late Glacial climatic fluctuations in Ecuador: glacier retreat during Younger Dryas time. Arctic and alpine research, 496-501.

Kaser, G., 1999. A review of the modern fluctuations of tropical glaciers. Global and Planetary Change 22, 93-103.

Kaser, G., Osmaston, H., 2002. Tropical Glaciers. Cambridge University Press, Cambridge, UK.

Kelley, S.E., Kaplan, M.R., Schaefer, J.M., Andersen, B.G., Barrell, D.J., Putnam, A.E., Denton, G.H., Schwartz, R., Finkel, R.C. and Doughty, A.M., 2014. High-precision 10 Be chronology of moraines in the Southern Alps indicates synchronous cooling in Antarctica and New Zealand 42,000 years ago. Earth and Planetary Science Letters, 405, 194-206.

Kelly, M.A., Lowell, T.V., Applegate, P.J., Phillips, F.M., Schaefer, J.M., Smith, C.A., Kim, H., Leonard, K.C. and Hudson, A.M., 2015. A locally calibrated, late glacial 10 Be production rate from a low-latitude, high-altitude site in the Peruvian Andes. Quaternary Geochronology.

Lal, D., 1991. Cosmic ray labeling of erosion surfaces: in situ nuclide production rates and erosion models. Earth and Planetary Science Letters 104, 424-439.

Mercer, J.H., 1984. Simultaneous climatic change in both hemispheres and similar bipolar interglacial warming: Evidence and implications. American Geophysical Union.

Milankovitch, M., 1941. Kanon der Erdebestrahlung und seine Anwendung auf das Eiszeitenproblem. Königlich Serbische Akademie.

Mix, A.C., Bard, E. and Schneider, R., 2001. Environmental processes of the ice age: land, oceans, glaciers (EPILOG). Quaternary Science Reviews, 204, 627-657.

Monnin, E. et al., 2001. Atmospheric CO_2 concentrations over the last glacial termination. Science 291, 112-114.

Nishiizumi, K., Imamura, M., Caffee, M.W., Southon, J.R., Finkel, R.C., McAninch, J., 2007. Absolute calibration of 10Be AMS standards. Nuclear Instruments and Methods in Physics Research B 258, 403–413.

Pendleton, S.L., Ceperley, E.G., Briner, J.P., Kaufman, D.S. and Zimmerman, S., 2015. Rapid and early deglaciation in the central Brooks Range, Arctic Alaska. Geology, 43(5), 419-422.

Pubs.usgs.gov. (2016). USGS P 1386-I -- Peru - Cordilleras - Oriental. [online] Available at: http://pubs.usgs.gov/pp/p1386i/peru/orient.html [Accessed 21 Apr. 2016].

Putnam, A.E., Schaefer, J.M., Denton, G.H., Barrell, D.J., Birkel, S.D., Andersen, B.G., Kaplan, M.R., Finkel, R.C., Schwartz, R. and Doughty, A.M., 2013. The Last Glacial Maximum at 44 S documented by a 10 Be moraine chronology at Lake Ohau, Southern Alps of New Zealand. Quaternary Science Reviews, 62, 114-141.

Rodbell, D., Smith, J.A., Mark, B.G., 2009. Glaciation in the Andes during the Lateglacial and Holocene. Quaternary Science Reviews 28, 2165-2212.

Saltzman, B., Maasch, K., 1991. A first-order global model of late Cenozoic climatic change II. Further analysis based on a simplification of CO_2 dynamics. Climate Dynamics 5, 201-210.

Sandeman, H.A., Hanmer, S., Davis, W.J., Ryan, J.J. & Peterson, T.D. 2004. Whole-rock and Nd isotopic geochemistry of Neoarchaean granitoids and their bearing on the evolution of the Central Hearne supracrustal belt, Western Churchill Province, Canada, Precambrian Research, vol. 134, no. 1, 143-167.

Science.purdue.edu, 2016. Purdue University :: PRIME Lab. [online] Available at: http://science.purdue.edu/primelab/ [Accessed 28 Feb. 2016].

Schaefer, J.M., Denton, G.H., Kaplan, M., Putnam, A., Finkel, R.C., Barrell, D.J.A., Andersen, B.G., Schwartz, R., Mackintosh, A., Chinn, T., Schlucter, C., 2009. High-frequency Holocene glacier fluctuations in New Zealand differ from the northern signature. Science 324, 622–625.

Shakun, J.D., et al., 2012. Global warming preceded by increasing carbon dioxide concentrations during the last deglaciation. Nature 484, 49-54.

Shakun, J.D., Clark, P.U., He, F., Lifton, N.A., Liu, Z. and Otto-Bliesner, B.L., 2015. Regional and global forcing of glacier retreat during the last deglaciation. Nature communications, 6.

Smith, Jacqueline A., Bryan G. Mark, and Donald T. Rodbell., 2008. The Timing and Magnitude of Mountain Glaciation in the Tropical Andes. Journal of Quaternary Science 23.6-7, 609-34.

Smith, J.A., Seltzer, G.O., Farber, D.L., Rodbell, D.T. and Finkel, R.C., 2005. Early local last glacial maximum in the tropical Andes. Science, 308(5722), 678-681.

Sobolev, S.V. and Babeyko, A.Y., 2005. What drives orogeny in the Andes?. Geology, 33(8), 617-620.

Stone, J.O.H., 2000. Air pressure and cosmogenic isotope production. Journal of Geophysical Research 105, 23753–2375

Thiel, M., Macaya, E.C., Acuna, E., Arntz, W.E., Bastias, H., Brokordt, K., Camus, P.A., Castilla, J.C., Castro, L.R., Cortes, M. and DUMONT, C.P., 2007. The Humboldt Current System of northern and central Chile: oceanographic processes, ecological interactions and socioeconomic feedback. Oceanography and Marine Biology, 45, 195-344.

Vuille, Mathias, et al., 2008. Climate change and tropical Andean glaciers: Past, present and future. Earth-science reviews 89.3, 79-96.

Yue, J. et al., 2015. Increasing carbon dioxide concentration in the upper atmosphere observed by SABER. Geophysical Research Letters 42, 7194-7199.

Zech, R., Kull, C., Kubik, P.W. and Veit, H., 2007. LGM and Late Glacial glacier advances in the Cordillera Real and Cochabamba (Bolivia) deduced from ^{10}Be surface exposure dating. Climate of the Past Discussions, 3(3), 839-869.

Appendix A

Extraction of Be from Quartz for Isotopic Analysis

Version:
This is Perry Spector's version as of November 2013 modified by Brenda Hall in September 2014, and eventually stripped down by Gordon Bromley in 2016. This version is based on instructions created by John Stone and Greg Balco.

References:
The cation exchange procedure is based on one developed by Bob Ditchburn of IGNS Inc., New Zealand.

Ditchburn, R. G. and N. E. Whitehead (1994) The separation of 10Be from silicates. 3d Workshop of the South Pacific Environmental Radioactivity Association, 4-7.

Ditchburn, R. G., I. J. Graham, and A. Zondervan (2000) Analytical methods for measuring Be and U-Th isotopes in loess. Institute of Geological and Nuclear Sciences science report 2000/09. Lower Hutt: Institute of Geological and Nuclear Sciences. 10p.

Steps:

1. Aluminum check for quartz purity
    a. Check trace-element content of quartz before dissolving it for ^{10}Be analysis with ICP optical emission spectroscopy (ICP-OES)
    b. Al-check preparation
        i. Use clean spatula to transfer 0.05-0.35 g into Teflon beaker
        ii. Add small amount of 1% HNO_3 to wet grains, place on hotplate in fume hood
        iii. Get clean 100ml reagent beaker, pour 2-3 mL of full-strength HF into reagent beaker
        iv. Add 2-3 mL of HF to each sample
        v. Add 1 ml of 8% H_2SO_4 to each beaker, set hotplate to 200 ^oF
        vi. After one hour, set hotplate to 275 ^oF for overnight drying into H_2SO_4 droplets, cool samples after drying
        vii. If sample forms an insoluble and solid cake precipitate, discard sample
        viii. Add 5 mL of 1% HNO_3 to each beaker, cap, and weigh for ICP analysis
    c. Provide HF treatment to clean quartz of high concentrations of impurities
        i. Re-clean and reprocess problematic samples
2. Beryllium chemistry
    a. Sample weighing
        i. Estimate the necessary sample amount to predict $^{10}Be/^{9}Be$ ratios (aim for ratios > 10^{-13})
        ii. Weigh 125 mL or 250 mL Teflon bottle without sample, then again with sample
        iii. Use 1% HNO_3 from wash bottle to wash grains from bottle mouth and sides, fully wet the grains

b. Carrier addition
    i. Record concentration of Be bottle, invert to homogenize, and weigh for initial weight
    ii. Load the 0 - 1 mL pipette with a clean tip, adjust it to deliver carrier containing ~250 μg Be. Don't contaminate the carrier
    iii. Open sample bottle, pipette carrier into sample without leaving a drop in the tip, and avoid contact with sample bottle
    iv. Recap carrier, re-weigh, record weights, and repeat process
c. Dissolution
    i. With protective gear on, add 5 mL of AR grade HF in each sample bottle for each gram of quartz, never shake bottle
    ii. Recap each bottle securely with vented caps, place on hotplate
    iii. After reaction is completed, set hotplate to "warm" and gradually increase temperature to 95 ºC over 24 hours until samples dissolve
d. Dry-down, cation removal, and chloride conversion of main sample
    i. Dry vessels on hotplate and evaporate at ~140°C with the hotplate tilted slightly
    ii. Re-dissolve samples in ~2-3 mL 6M HCl, wet and dry down again
    iii. Repeat HCl addition and dry down with 2 mL HCl
    iv. Take back up in ~3 mL 6M HCl
e. Fe, Ti clean-up (anion exchange columns)
    i. Load a column rack with a set of large anion exchange columns
    ii. Place waste beaker under each column
    iii. Run a few mL of MQ water smoothly down the wall of the column, and before it drains, pipette in a loose slurry of anion exchange resin
    iv. Build the resin beds up to 2 mL
    v. Wash the resin bed with 5 times its volume of 0.3 M HCl, let it drain
    vi. Condition the resin with 3 bed volumes of 6M HCl carefully
    vii. Remove waste beakers and replace with labelled 28 mL Teflon vials
    viii. Using a separate disposable pipette for each sample, load the sample solutions onto the columns
    ix. Add 1 mL 6M HCl to each beaker as rinse, allow solutions to fully drain
    x. Elute Be from the columns by adding 3 times the bed volume of 6M HCl
    xi. Remove vials containing Be and set aside
    xii. Discard resin, wash columns, rinse and discard sample and pipettes, wash sample transfer containers
f. Conversion to sulfate
    i. Add 1 mL of 0.5 M H_2SO_4 to each vial and dry on the hotplate at ~135°C
    ii. Once dried down, cool the beakers and add 2 drops of ~2% H_2O_2

iii. Add 2-3 mL of MQ water with disposable pipette, reheat the vials and dry
iv. Cool, repeat the H_2O_2 /H_20 addition, and dry the samples
v. Take the samples up in 3-4 mL of MQ water, containing a couple drops of 30% H_2O_2 or trace of 2% H_2O_2, warm them to get them back in solution

g. Be separation (cation exchange columns)
i. Load a column rack with small (~11 mL total volume) Bio-Rad columns, with waste beakers under columns
ii. Using a disposable pipette, add 2 mL of DOWEX-50 X8 200-400# cation exchange resin (can use AGI 50Wx8) to each column
iii. Clean resin by filling each column headspace with 3 M HCl, let it drain
iv. Make up a beaker of ~ 0.2 M H_2SO_4 containing a few drops of 30% peroxide, mix well
v. Condition the columns by filling the headspace with this solution, allow it to drain through
vi. Discard any leftover conditioning acid in the waste container, and replace it with 0.5 M H_2SO_4 containing a dash of 2% H_2O_2
vii. Load each sample with clean disposable pipette
viii. While the sample solutions run in, add 1 mL of 0.5 M H_2SO_4/trace of 2% H_2O_2 to each beaker as a rinse, let drain
ix. Gradually add 10 mL (5 bed volumes) of 0.5 M H_2SO_4/trace H_2O_2 to each column
x. Remove the waste beakers and replace them with labelled 28 mL Teflon vials
xi. Elute Be from the columns with 10 mL (5 bed volumes) of 1.2 M HCl
xii. Let columns drain, remove vials and add 5 drops of 8 M HNO_3 to each vial, then dry them on a hotplate at ~135°C

h. Be recovery and storage
i. For each sample, label a clean 15 mL screw cap centrifuge tube
ii. Cool dried samples and pipette 2 mL of 1% HNO_3 into each vial
iii. Carefully tip each solution into its correct centrifuge tube
iv. Pipette a second 2 mL aliquot of 1% HNO3 into each vial as a rinse
v. Warm it, run it around the beaker and add it to the correct centrifuge tube
vi. Cap the centrifuge tubes and store for hydroxide precipitation

3. Be recovery and cathode preparation for AMS analysis

Note: *Precipitate, ignite, and pack Be samples shortly before the accelerator run in which they will be measured. Cathodes packed in advance of a run (or cathodes which have to be stored after a cancelled run) should be stored in the desiccator*

a. Beryllium Hydroxide Precipitation

i. Mix a solution of 1-part ammonium hydroxide with 2 parts MQ water and mix well
ii. Add ~6 drops to a sample, close the centrifuge tube, and use the vortex mixer to homogenize
iii. Continue to add ~5 drops at a time and spin with the vortex mixer until a white, almost translucent precipitate forms
iv. The pH should be ~7-8 (though it can be a bit higher) for $Be(OH)_2$ to precipitate
v. After all samples have precipitated Be(OH)2, wait 10-20 minutes for the precipitate to flocculate
vi. Centrifuge at 2,600 RPM for 5 minutes
vii. Pour the supernatant into the sink, retaining the white hydroxide gel
viii. Fill to 5 mL with MQ water, spin again on the vortex mixer, wait for the precipitate to flocculate, centrifuge again, and pour off the liquid
ix. Label centrifuge-tube caps, place the centrifuge tubes in a rack laid on its side (though prop up one side of the rack with the centrifuge caps so that the tubes are at a shallow angle) in the oven set to the normal temperature (70°C) – Takes overnight

b. Conversion to beryllium oxide
i. Cut 4x4 in. weighing paper into four (2x2 in.) pieces until there is at least one for each sample
ii. Place a piece of paper down in the laminar flow hood with a chemwipe on top of that
iii. Fold the weighing paper in order to make a small scoop, place on chemwipe to catch dried hydroxide precipitate – Don a mask
iv. Wave the test tube in front of the ionizer to reduce static before tipping it onto folded weighing paper
v. Transfer it to one of the clean pre-labelled nitric-etched glass vials, cover with parafilm, repeat process for each sample
vi. Place crucibles in block heater, taking care to put the first sample in spot A, record position of samples
vii. Fetch a propane torch, stand and crucible tongs and set them up in the hood well away from the walls - Light the torch
viii. After removing the parafilm from the vial, grasp the vial with the tongs about halfway up
ix. Wave the crucible through the flame cautiously at first
x. Once the sample begins to glow, hold it in the flame for 30 to 40 seconds more
xi. Remove it from the heat and place it back in the same spot in the heating block in the hood to cool

c. Niobium addition
i. Clean the niobium scoop (#1 curette) with a chemwipe and alcohol
ii. Set up a large chemwipe in the downflow hood, along with the sample vials and the niobium with scoop

iii. Make sure samples are cool
iv. For each sample - Add 1 rounded scoop of niobium powder
v. Add a clean drill bit to the tube, and then label a cathode and cathode container with the sample name
vi. Record cathode number, place the vial in the cathode and the cathode in the cathode container
vii. Discard test tube and chemwipe in Be waste bag

d. Beryllium cathode packing
   i. First, prepare the glove box, wipe out the floor of the box with DI water, which you should leave in the box - Make sure the Be waste container has a bag with enough room for chemwipes and vials
   ii. Place chemwipes, ionizer, hammer, and the rack of cathodes inside of the box
   iii. Put on sleeves and close the sample door from the inside
   iv. Lay down a chemwipe on the bottom of the box and place a cathode onto it
   v. Remove the vial and begin crushing the BeO pellet with the drill bit and mixing it with the niobium powder, gather all the powder in the very bottom
   vi. Gently tap any remaining sample onto the cathode GENTLY using the side of the hammer
   vii. Place the empty vial on the chemwipe - Continue to tap around the sides of the cathode until all the powder has made it into the hole
   viii. Place the business end of the drill bit into the cathode hole and press down until it slides in
   ix. Firmly tap the bit until it you hear a solid, sturdy sound and are certain that it has been sufficiently packed down - Remove the drill bit
   x. Gently upend cathode on the chemwipe to remove any loose powder
   xi. Put the cathode into the cathode container and close the cap
   xii. Place the drill bit into the small beaker of alcohol with the business end in the liquid
   xiii. Between each sample be sure to wipe down the central floor of the box to prevent cross-contamination

Table 2. Sample locations and attributes, along with added ^{9}Be carrier information.

Sample	Latitude	Longitude	Quartz weight (g)	^{9}Be carrier weight (g)	^{9}Be carrier concentration (ppm)	Boulder dimensions (cm) L*W*H
NT-11-01	-14.16354	-70.26168	2.9277	0.3920	635	300*220*120
NT-11-02	-14.16417	-70.26357	2.0497	0.3986	635	120*100*85
NT-11-03	-14.16415	-70.26368	2.4337	0.3895	635	220*130*60
NT-11-06	-14.16158	-70.27045	2.8847	0.3901	635	90*75*45
NT-11-10	-14.16156	-70.26956	4.3212	0.3905	635	320*200*155
NT-11-11	-14.16189	-70.26817	1.4003	0.3055	813	80*75*60
NT-11-12	-14.16192	-70.26713	2.2245	0.3992	635	260*40*40
NT-11-14	-14.16130	-70.26697	10.076	0.3992	635	160*130*65
NT-11-15	-14.16121	-70.26668	2.6018	0.3989	635	120*110*60
NT-11-19	-14.15710	70.26973	12.502	0.4011	635	270*250*140

NT-11-01

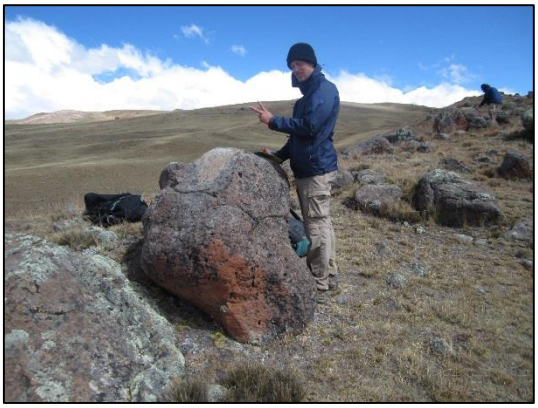

NT-11-02

NT-11-03

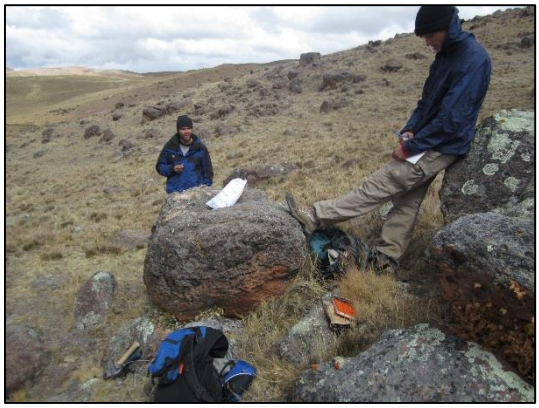

NT-11-06

NT-11-10

NT-11-11

NT-11-12

NT-11-14

NT-11-15

NT-11-19